

1

2

3

4

5 **Protein homeostasis from diffusion-dependent control of protein**  
6 **synthesis and degradation**

7

8 Yuping Chen<sup>1,3,4</sup>, Jo-Hsi Huang<sup>1,3</sup>, Connie Phong<sup>1</sup>, and James E. Ferrell, Jr.<sup>1,2,4,5</sup>

9

10 <sup>1</sup>Dept. of Chemical and Systems Biology, Stanford University School of Medicine, Stanford CA  
11 94305

12 <sup>2</sup>Dept. of Biochemistry, Stanford University School of Medicine, Stanford CA 94305

13 <sup>3</sup>These authors contributed equally

14 <sup>4</sup>Corresponding authors

15 <sup>5</sup>Lead contact

16

17 **Contact info**

18 \*Correspondence: Yuping Chen [cyp7cn@gmail.com](mailto:cyp7cn@gmail.com) and James E. Ferrell, Jr.  
19 [James.ferrell@stanford.edu](mailto:James.ferrell@stanford.edu).

20

## 21 **Summary**

22 It has been proposed that the concentration of proteins in the cytoplasm maximizes the speed of  
23 important biochemical reactions. Here we have used the *Xenopus* extract system, which can be  
24 diluted or concentrated to yield a range of cytoplasmic protein concentrations, to test the effect of  
25 cytoplasmic concentration on mRNA translation and protein degradation. We found that protein  
26 synthesis rates are maximal in ~1x cytoplasm, whereas protein degradation continues to rise to  
27 an optimal concentration of ~1.8x. This can be attributed to the greater sensitivity of translation  
28 to cytoplasmic viscosity, perhaps because it involves unusually large macromolecular complexes  
29 like polyribosomes. The different concentration optima sets up a negative feedback homeostatic  
30 system, where increasing the cytoplasmic protein concentration above the 1x physiological level  
31 increases the viscosity of the cytoplasm, which selectively inhibits translation and drives the  
32 system back toward the 1x set point.

## 33 **Keywords**

34 Cytoplasmic concentration, protein homeostasis, diffusion control, maximal speed conjecture,  
35 protein synthesis and degradation, viscosity, molecular crowding, *Xenopus* egg extract

## 36 **Introduction**

37 The cytoplasm is crowded with macromolecules, with proteins being the most abundant class. In  
38 total, proteins constitute about 82% of the dry mass of a mammalian cell (Oh et al., 2022) and  
39 about 55% of an *E. coli* cell (Milo et al., 2009), and the cytoplasmic concentration of protein  
40 ranges from about ~75 mg/mL in mammalian cell lines (Liu et al., 2022) and *Xenopus* egg  
41 extracts (Green, 2009; Murray, 1991) to 200-320 mg/mL in *E. coli* (Elowitz et al., 1999;  
42 Zimmerman and Trach, 1991). Assuming an average protein density of 1.35 g/mL, this means  
43 that the volume fraction of a cell occupied by protein is ~6% to 25%, and the macromolecular  
44 excluded volume is higher still. Although protein concentration transiently decreases during  
45 mitosis (Son et al., 2015; Zlotek-Zlotkiewicz et al., 2015), for a given cell type, the concentration  
46 of macromolecules in the cytoplasm is tightly regulated and remarkably constant (Delarue et al.,  
47 2018; Liu et al., 2022; Neurohr and Amon, 2020; Oh et al., 2022).

48 This brings up two basic questions: why is the cytoplasmic protein concentration as high as it is,  
49 and no higher, and what mechanisms set and maintain this concentration? It has been conjectured

50 that the normal cellular protein concentration maximizes the rates of important biochemical  
51 reactions, with there being a trade-off between the effects of concentration on enzyme-substrate  
52 proximity and viscosity (Dill et al., 2011). This conjecture assumes that these critical reactions  
53 are sensitive to the viscosity of the medium because the collision frequency of their reactants  
54 depends upon viscosity. Note, however, that decades of in vitro work has indicated that almost  
55 all enzymes are reaction-limited, not diffusion-limited (Bar-Even et al., 2011), so that changes in  
56 diffusion might be expected to have minimal effect on the rates of most enzyme reactions. That  
57 said, there are examples of protein-mediated processes that are markedly inhibited by increased  
58 viscosity (Alric et al., 2022; Drenckhahn and Pollard, 1986; Molines et al., 2022; Tan et al.,  
59 2013), and the simplest explanation for this is that they are diffusion controlled. Thus, the  
60 maximal speed conjecture remains an intriguing possibility.

61 Here we set out to directly test the conjecture experimentally. We chose to use the *Xenopus* egg  
62 extract system, an undiluted cell-free living cytoplasm, for these studies because they allow easy,  
63 direct manipulation of the concentration of cytoplasmic macromolecules. Although *Xenopus*  
64 extracts are an in vitro system, they carry out the complex biological functions of an intact  
65 *Xenopus* egg or embryo remarkably faithfully. For example, extracts can self-organize into  
66 sheets of cell-like structures whose overall architecture closely resembles that of embryonic  
67 blastomeres (Cheng and Ferrell, 2019; Gires et al., 2023; Mitchison and Field, 2021). If supplied  
68 with sperm chromatin, extracts can organize a functional nucleus and carry out DNA replication.  
69 Indeed, extracts can perform full cell cycles, complete with replication, mitosis, and reductive  
70 division of the cell-like cytoplasmic structures (Afanzar et al., 2020; Cheng and Ferrell, 2019;  
71 Fang and Newport, 1991; Murray and Kirschner, 1989).

72 The processes we chose to examine were protein synthesis and degradation, which are not only  
73 potentially affected by the cytoplasmic protein concentration, but also directly involved in  
74 determining the protein concentration. *Xenopus* extracts can carry out protein synthesis from  
75 their own stores of mRNAs or from added synthetic mRNAs (Kanki and Newport, 1991;  
76 Minshull et al., 1989; Ruderman et al., 1979), and they degrade both endogenous proteins (most  
77 notably the various substrates of the APC/C) (Kamenz et al., 2021; King et al., 1996) and added  
78 probe proteins [the present work]. In some ways, both *Xenopus* extracts and the eggs from which  
79 they are derived represent unusual systems for studies of protein control. Transcription is largely

80 absent from fertilized eggs and developing embryos until the midblastula transition (Amodeo et  
81 al., 2015; Newport and Kirschner, 1982a, b), and the mRNA content is unchanging throughout  
82 the cleavage stages of embryogenesis. In addition, although translational control is critical during  
83 oocyte maturation and immediately after fertilization (Fox et al., 1989; Meneau et al., 2020; Paris  
84 et al., 1988; Richter et al., 2007; Rosenthal et al., 1983), it appears not to be important during  
85 much of embryogenesis (Peshkin et al., 2015). In other ways, the dynamics of proteins in  
86 *Xenopus* extracts are typical of animal cells. Common mammalian cell lines have protein  
87 concentrations of about 75 mg/mL (Liu et al., 2022), as do *Xenopus* extracts (Murray, 1991), and  
88 the median protein half-lives in *Xenopus* extracts (Peshkin et al., 2015) and mouse NIH3T3 cells  
89 (Schwanhausser et al., 2011) are almost identical. The simplicity, manipulability, and  
90 verisimilitude of the extract system makes it an attractive choice for the present studies of how  
91 protein synthesis and degradation are affected by the cytoplasmic concentration.

92 In this study, we directly manipulated the cytoplasmic macromolecule concentration and  
93 viscosity of *Xenopus* egg extracts and assessed the immediate effects on protein synthesis and  
94 degradation. We found that translation rates were maximal in 1x cytoplasmic extracts; translation  
95 initially increased with cytoplasmic concentration, but then sharply decreased above 1x. Thus,  
96 translation is an example of a process whose speed is in fact maximized at the normal  
97 concentration of cytoplasmic macromolecules. In contrast, degradation rises with cytoplasmic  
98 concentration until the concentration reaches almost 2x. The different concentration optima can  
99 be explained by the sensitivities of the processes to viscosity; the viscogen Ficoll 70 was found  
100 to be a more potent inhibitor of protein synthesis than of protein degradation. The differential  
101 sensitivity of protein synthesis and protein degradation to viscosity provides a simple mechanism  
102 for ensuring long-term protein concentration homeostasis.

103

## 104 **Results**

### 105 ***Xenopus* egg extracts are robust towards cytoplasmic dilution and concentration.**

106 The most commonly used types of extract are CSF (cytostatic factor)-arrested extracts,  
107 interphase-arrested extracts, and cycling extracts (Cheng and Ferrell, 2019; Dunphy et al., 1988;  
108 Murray, 1991; Newport and Spann, 1987). In pilot experiments we found that cycling extracts

109 were the most reliable and longest lived, and so they were chosen for most of the experiments  
110 that follow. One caveat is that previous work has shown that translation rates vary between  
111 interphase and M-phase (Kanki and Newport, 1991), raising the concern that the time course of  
112 protein synthesis would be characterized by alternations between different rates. This proved not  
113 to be the case, possibly because mitosis sweeps through the extract in spatial waves (Chang and  
114 Ferrell, 2013) (see Movies S1 and S2), so that both mitotic and interphase rates would probably  
115 contribute to the measured rate of synthesis at all time points.

116 To alter the macromolecular concentration of cycling extracts, we used a spin-column with a 10  
117 kilodalton (kDa) cutoff to produce a cytosolic filtrate and a cytoplasmic concentrate (Figure 1B).  
118 The filtrate was found to be essentially protein-free by Bradford assay as well as by gel  
119 electrophoresis and Trihalo compound or Coomassie staining (Figure 1C and S1). The retentate  
120 was on average 2-fold concentrated compared to the starting cytoplasm by Bradford assay  
121 (Figure 1C). We then diluted either the starting 1x extract or the 2x retentate with the filtrate to  
122 generate extracts with a range of cytoplasmic macromolecule concentrations (Figure 1D, E).

123 We first examined the effects of concentration on two basic aspects of the extract's function: its  
124 ability to self-organize and to cycle. The extract's gross organization was found to be remarkably  
125 robust to cytoplasmic dilution (Figure 1D, E). Using a microtubule stain, SiR-tubulin, cell-like  
126 compartments (Afanzar et al., 2020; Cheng and Ferrell, 2019) were found to form even when the  
127 extract was diluted to as low as 0.3x (Figure 1D, E, and Movies S1-S3), in general agreement  
128 with a previous report (Cheng and Ferrell, 2019), and to partially organize, with small asters,  
129 even at 0.2x the normal cytoplasmic concentration (Movie S3). By following microtubule  
130 polymerization and depolymerization, cell cycles were detected down to dilutions of 0.2x, and  
131 the oscillations persisted for at least 14 hours with more than 10 complete periods (Figure 1C, D,  
132 Movies S1-S3). In agreement with a previous study (Jin et al., 2022), the diluted extracts did not  
133 show signs of significant cell cycle defects except that the duration of interphase and the cell  
134 cycle period increased with increasing dilution.

135 On the other hand, the 2x retentate was stickier and more viscous than a 1x extract. Cell-like  
136 compartments failed to form at concentrations higher than 1.4x (Figure 1E), and the cell cycle  
137 appeared to be arrested above 1.4x. Nevertheless, when a 2x extract was diluted to 1.4x or less,  
138 cell-like compartment formation was restored, and the cell cycle behavior was almost normal

139 (Figure 1E), although dilutions from the 2x retentate had slightly longer interphases and were  
140 slightly more susceptible to apoptosis than dilutions from a 1x extract (Figures 1D and E).  
141 Overall, extracts were more sensitive to being concentrated than diluted, but even so, extracts  
142 were able to carry out grossly normal self-organization and cycling over a wide range of  
143 cytoplasmic concentrations.

#### 144 **Protein synthesis peaks at a 1x cytoplasmic concentration.**

145 To measure the protein synthesis rate, we added an mRNA for eGFP and monitored fluorescence  
146 as a function of time. In pilot experiments, we titrated the mRNA concentration and found that  
147 we could obtain a satisfactory signal without saturating the translation machinery using a  
148 concentration of 2.5 ng/ $\mu$ L (Figure 2A). We then recorded time courses of eGFP fluorescence  
149 intensity for diluted and concentrated extracts all with the same 2.5 ng/ $\mu$ L concentration of  
150 mRNA for eGFP, and calculated translation rates from the linear portion of the time course  
151 (Figure 2B). Figure 2C summarizes the data as directly obtained, with equal concentrations of  
152 mRNA at each dilution but differing concentrations of the translation machinery. In principle,  
153 calculated rates can be plotted against either relative cytoplasmic concentration using the average  
154 fold relation from multiple experiments (Figure 1C) or absolute protein concentration measured  
155 for each experiment. However, we observed that absolute protein concentration for individual  
156 experiments was no better at addressing the variability among experiments than relative  
157 cytoplasmic concentration (Figure S2). Furthermore, relative cytoplasmic concentration provides  
158 a more straightforward theoretical treatment, as discussed later. Therefore, we opted to use  
159 relative cytoplasmic concentration in instances where both relative cytoplasmic concentration  
160 and protein concentration were viable options. Translation increased with cytoplasmic  
161 concentration to a maximum at  $\sim 0.75x$  and fell thereafter. To relate this to endogenous  
162 translation, given that the endogenous mRNAs would vary with concentration just as the  
163 translation machinery does, we calculated an inferred endogenous translation rate, taken as the  
164 observed translation rate multiplied by the cytoplasmic concentration. This is shown in Figure  
165 2D; maximal translation was obtained at a cytoplasmic concentration of  $\sim 1x$ . We also calculated  
166 the translation rate normalized for both equal ribosome concentration and equal mRNA  
167 concentration, by dividing the raw translation rates by the cytoplasmic concentration (Figure 2E).  
168 This provides an estimate of how the specific activity of the translation machinery is affected by

169 cytoplasmic concentration. The inferred specific activity fell markedly with increasing  
170 cytoplasmic concentration above 0.5x; below that there was too much variability to draw  
171 conclusions. These findings show that protein synthesis is fastest in 1x cytoplasm, as predicted  
172 by the maximal speed conjecture (Dill et al., 2011), and suggest that protein synthesis is inhibited  
173 when the cytoplasmic viscosity is higher than normal. This latter point is explored further below.

174 As a second way of gauging the translation rate, we added equal concentrations of <sup>35</sup>S-  
175 methionine to extracts with a range of cytoplasmic concentrations and no added exogenous  
176 mRNA, and measured <sup>35</sup>S incorporation into TCA-precipitable material. Figure 2F shows that  
177 incorporation increased linearly with time through 75 min, and that the protein synthesis  
178 inhibitor cycloheximide blocked this incorporation. Translation peaked at a cytoplasmic  
179 concentration of ~0.8x (Figure 2G). Overall the dependence of translation on cytoplasmic  
180 concentration was very similar to that seen with eGFP (Figure 2D and 2G), and again the  
181 inferred specific activity of the translation machinery fell with cytoplasmic concentrations above  
182 ~0.5x (Figure 2H). Thus the effects of cytoplasmic concentration seen with eGFP translation  
183 appear to be applicable to translation from endogenous mRNAs as well.

#### 184 **Protein degradation peaks at a higher cytoplasmic concentration.**

185 As a first measure of protein degradation, we made use of an exogenous protein substrate, a  
186 heavily BODIPY (boron-dipyrromethene)-labeled BSA, DQ-BSA (for dye-quenched bovine  
187 serum albumin). This protein becomes fluorescent during degradation because the BODIPY  
188 groups become dequenched. We carried out titration experiments, which showed that an  
189 approximately linear response could be obtained with a DQ-BSA concentration of 5 µg/mL  
190 (Figure 3A, B). This concentration was then used for experiments with extracts diluted to various  
191 extents. As shown in Figure 3C, the rate of DQ-BSA dequenching increased with the  
192 concentration of macromolecules and peaked at about 1.6x. The proteasome inhibitor MG132  
193 blocked this dequenching, indicating that dequenching was largely due to proteasomes rather  
194 than lysosomes. As we did for eGFP synthesis, we also multiplied the rate data by the extract  
195 concentration to infer a degradation rate for endogenous proteins, where both the substrate and  
196 the proteolysis machinery would be affected by cytoplasmic concentration; this shifted the  
197 activity peak to ~1.8x (Figure 3D). Note that by paired *t*-test, the average for the 1.8x data was  
198 not significantly higher than the average for the 2x data ( $p = 0.26$  for a one-tailed *t*-test), so the

199 optimal cytoplasmic concentration for DQ-BSA dequenching may actually be higher than 1.8x.  
200 The specific activity calculation (Figure 3E) showed that the enzyme activity fell above ~1.4x  
201 cytoplasmic concentration. At lower cytoplasmic concentrations, the relationship between this  
202 gauge of activity and concentration was complicated; perhaps simple bimolecular kinetics do not  
203 pertain in this regime.

204 As a second measure of protein degradation, we used a securin-CFP fusion protein as a reporter.  
205 Securin is a cell cycle protein known to be targeted for proteasome-mediated protein degradation  
206 by the anaphase promoting complex/cyclosome (APC/C) in late mitosis. We measured the decay  
207 of securin-CFP fluorescent intensity and calculated the degradation rate (Kamenz et al., 2021)  
208 for each of the dilution conditions (Figure 3F). As was the case with DQ-BSA dequenching, the  
209 protein degradation rate peaked at a ~1.6x cytoplasmic macromolecular concentration (Figure  
210 3G), and the inferred rate for a substrate being diluted along with the degradation machinery  
211 peaked at 1.8x (Figure 3H). Again, by paired *t*-test, the average for the 1.8x data was not  
212 significantly higher than the average for the 2x data ( $p = 0.34$  for a one-tailed *t*-test), so the  
213 optimal cytoplasmic concentration for securin-CFP degradation may be higher than 1.8x. The  
214 inferred specific activity for securin-CFP degradation fell steadily with concentration (Figure 3I).  
215 Thus, by both measures, protein degradation rates were maximal at a cytoplasmic concentration  
216 of about 1.8x, higher than the optimal concentration for protein synthesis.

### 217 **Viscosity affects protein translation rate and, to a lesser extent, protein degradation.**

218 The decrease in translation at high cytoplasmic macromolecule concentrations suggests that  
219 translation is diffusion-controlled in a viscous cytoplasm, and that concentrated cytoplasm has a  
220 higher viscosity that reduces the molecular movement necessary for the translation reaction. To  
221 test these ideas, we first measured how diffusion coefficients vary with cytoplasmic  
222 concentration. We used single particle tracking of fluorescently labeled PEGylated 100 nm  
223 diameter polystyrene beads, which are comparable in size to some of the large complexes  
224 involved in translation (Figure 4A). In 1x extracts, the motion of the beads was subdiffusive,  
225 with the diffusivity exponent  $\alpha$  to be  $0.88 \pm 0.06$  (means  $\pm$  S.E.) (Figure 4B, C). We calculated  
226 an average effective diffusion coefficient  $D$  from a fit of the random walk diffusion equation to  
227 the data over a time scale of 1 s. This was found to be  $0.36 \pm 0.23 \mu\text{m}^2/\text{s}$  (means  $\pm$  S.E.), in good

228 agreement with previous studies (Delarue et al., 2018; Huang et al., 2022). There was substantial  
229 variability from position to position in the speed of diffusion (Figure 4B, insets, and 4C).  
230 Similarly high variability has been reported for the diffusion of genetically-encoded  
231 nanoparticles expressed in *S. pombe* (Garner et al., 2023), which is thought to reflect the  
232 heterogeneity of the cytoplasmic environment.

233 The effective diffusion coefficient for the 100 nm beads varied dramatically with cytoplasmic  
234 concentration; it was ~11x higher in filtrate (0x cytoplasm) compared to 1x extracts, and ~11x  
235 lower in 2x extracts. The measured diffusion coefficients obeyed Phillies's law (Phillies, 1986;  
236 Phillies, 1988):

$$237 \quad D[\phi] = D[0]e^{-\mu\phi}, \quad [\text{Eq. 1}]$$

238 where  $D[\phi]$  is the diffusion coefficient at a relative cytoplasmic concentration  $\phi$ ,  $D[0]$  is the  
239 diffusion coefficient in filtrate, and  $\mu$  is a scaling factor that depends upon the size of the probe.  
240 A similar relationship between diffusion coefficients and macromolecular concentration has been  
241 observed for large multimeric protein complexes (Alric et al., 2022; Molines et al., 2022).  
242 Similarly, the scaling factor varied approximately linearly with the measured size of the beads  
243 (Figure 4D) (Alric et al., 2022). Thus, diffusion was markedly affected by changing the  
244 cytoplasmic macromolecule concentration over a 0x to 2x range, and the changes were greatest  
245 for large probe particles.

246 Next, we diluted extracts to 0.7x, 0.8x, or 0.9x, and altered the cytoplasmic viscosity by adding  
247 Ficoll 70, a protein-sized (70 kDa) carbohydrate that can act both as a crowding agent and a  
248 viscogen (Figure 4G). The effective diffusion coefficients were found to decrease with  
249 increasing Ficoll concentration; 6% Ficoll 70 decreased the diffusion coefficient for a 40 nm  
250 bead by a factor of 33, and 2-3% Ficoll 70 yielded diffusion coefficients comparable to those  
251 measured in 2x cytoplasm. Thus, Ficoll can be used to bring about the marked changes in  
252 viscosity seen when cytoplasm is concentrated, without changing protein concentration.

253 We therefore asked whether this range of Ficoll 70 concentrations would inhibit protein  
254 synthesis and degradation. Note that Ficoll might be expected to have either of two opposite

255 effects on enzyme reaction rates: by acting as a crowding agent, it increases the concentrations of  
256 the reactants and thus could increase the rate of a reaction; but by acting as a viscogen, it could  
257 slow protein motions and decrease in the reaction rate. In vitro studies have shown that either of  
258 these effects can predominate (Aoki et al., 2013; Minton, 2001; Tan et al., 2013). We found that  
259 the rate of translation of eGFP monotonically decreased with increasing Ficoll 70 concentration,  
260 with an IC50 of ~2-3% (Figure 4H). Diffusion coefficients in these Ficoll-supplemented 0.7x to  
261 0.9x extracts supplemented with 2-3% Ficoll 70 were similar to those seen in 2x extracts with no  
262 Ficoll. Thus protein synthesis is sensitive to viscosity over a range relevant to the cytoplasmic  
263 concentration/dilution experiments.

264 The rate of DQ-BSA unquenching was substantially less sensitive to viscosity (Figure 4I), with  
265 an IC50 greater than 6% Ficoll 70. Thus, both protein synthesis and protein degradation, as  
266 measured by the eGFP and DQ-BSA assays, are sensitive to the viscosity of the cytoplasm, with  
267 synthesis being more sensitive than degradation. This difference in sensitivity is sufficient to  
268 account for the different optimal cytoplasmic concentrations found for translation and  
269 degradation.

## 270 **A model for the effect of diffusion on reaction rates**

271 Final, we asked whether we could derive a simple model to account for the observed rates of  
272 protein translation and degradation as a function of cytosolic protein concentration. In particular,  
273 we wished to see if plausible assumptions could account for the biphasic nature of the curves,  
274 and to explore how differences in the kinetics of translation vs. degradation might account for the  
275 differences in their concentration optima.

276 We assume that the rate determining reaction for each process is a mass action bimolecular  
277 reaction:

$$278 \quad V = \frac{dP}{dt} = kE \cdot S \quad [\text{Eq 2}]$$

279 where  $V$  is the rate of the reaction,  $P$  is the product of the reaction,  $E$  is the enzyme,  $S$  the  
280 substrate, and  $P$  the product of the reaction. Alternatively, we could assume a two-step, saturable  
281 mechanism (see Supplementary Information), but the mass action treatment suffices for present

282 purposes and is simpler. The enzyme and substrate concentrations are linearly proportional to the  
283 relative cytoplasmic concentration  $\phi$ . We can therefore write:

$$284 \quad E[\phi] = \phi E[1] \quad [\text{Eq. 3}]$$

$$285 \quad S[\phi] = \phi S[1], \quad [\text{Eq. 4}]$$

286 where  $E[\phi]$  and  $S[\phi]$  are the enzyme and substrate concentrations at a relative cytoplasmic  
287 concentration of  $\phi$ , and  $E[1]$  and  $S[1]$  are the enzyme and substrate concentrations at a relative  
288 cytoplasmic concentration 1x. Substituting into Eq. 2 yields:

$$289 \quad V = k\phi^2 E[1]S[1]. \quad [\text{Eq. 5}]$$

290 Next we consider the dependence of the rate constant on the cytoplasmic protein concentration.  
291 From the Smoluchowski equation (Smoluchowski, 1917), the collision rate and the association  
292 rate constant  $k$  are proportional to the sum of the diffusion coefficients of  $E$  and  $S$ , and from  
293 Phillips's law (Eq. 1) (Phillies, 1986; Phillies, 1988), we take the diffusion coefficients to be  
294 negative exponential functions of the cytoplasmic protein concentration:

$$295 \quad k[\phi] \propto D_E[\phi] + D_S[\phi] = D_E[0]e^{-\mu_E\phi} + D_S[0]e^{-\mu_S\phi}, \quad [\text{Eq. 6}]$$

296 where  $D_E[0]$  and  $D_S[0]$  are the diffusion coefficients of the enzyme and the substrate at a  
297 cytoplasmic concentration of 0 (i.e. in filtrate), and the  $\mu$ 's are scaling factors. For the special  
298 case where either one diffusion coefficient is much smaller than the other, or the scale factors are  
299 equal, we can simplify this to:

$$300 \quad k[\phi] = k[0]e^{-\mu\phi}. \quad [\text{Eq. 7}]$$

301 Note that it is a bit awkward to consider a value of  $k$  at a relative cytoplasmic concentration of 0,  
302 since the reacting species are cytoplasmic macromolecules that are absent from the filtrate. We  
303 can avoid this by instead writing:

$$304 \quad k[\phi] = k[1]e^{-\mu(\phi-1)}. \quad [\text{Eq. 8}]$$

305 It follows that:

$$306 \quad V = k[1]E[1]S[1](\phi^2 e^{-\mu(\phi-1)}). \quad [\text{Eq. 9}]$$

307 Finally, we can make use of the fact that the scaling factor  $\mu$  is linearly proportional to the size of  
308 the diffusing particle  $d_p$ , and write an expression that explicitly acknowledges particle size:

$$309 \quad V = k[1]E[1]S[1](\phi^2 e^{-ad_p(\phi-1)}). \quad [\text{Eq. 10}]$$

310 where  $a$  is a new scaling factor that relates  $d_p$  to  $\mu$ . Eq. 10 describes how the rate of a mass  
311 action, bimolecular reaction whose reactants obey Phillip's law and mass would be expected to  
312 vary with the cytoplasmic macromolecule concentration and molecular diameter. If we measure  
313 rates in arbitrary units with the rate at  $\phi = 1$  taken as 1, then:

$$314 \quad V = \phi^2 e^{-ad_p(\phi-1)}. \quad [\text{Eq. 11}]$$

315 Note that we have an experimental estimate for  $a$  (which, from Figure 4F is  $0.018 \text{ nm}^{-1}$ ), leaving  
316 only one adjustable parameter,  $d_p$ , the macromolecular diameter. Eq. 11 defines a biphasic, non-  
317 monotonic curve (Figure 5A), and the larger the assumed macromolecular diameter, the further  
318 to the left the curve's maximum lies (Figure 5A). For a given value of  $d_p$ , the optimal  
319 cytoplasmic concentration is given by:

$$320 \quad \phi_{optimal} = \frac{2}{ad_p}. \quad [\text{Eq. 12}]$$

321 The experimentally observed rates for translation and degradation are well captured by Eq. 11,  
322 with the fitted values of  $d_p$  being  $104 \pm 2 \text{ nm}$  for translation and  $14 \pm 1 \text{ nm}$  for degradation  
323 (means  $\pm$  S.E.) (Figure 5C).

324 The result is a dynamical system that will be in steady state—the translation and degradation  
325 rates will be equal—at a relative cytoplasmic concentration of 1x. Moreover, the steady state is  
326 guaranteed to be stable. If the system is perturbed such that the cytoplasmic concentration  
327 exceeds 1x, then the degradation rate will rise and the translation rate will fall, driving the system  
328 back toward the 1x steady state (Figure 5C). Conversely, if the cytoplasmic concentration falls  
329 below 1x, the translation rate will exceed the synthesis rate, again driving the system back  
330 toward the physiological set point (Figure 5C).

## 331 Discussion

332 Here we have tested the hypothesis that the concentration of macromolecules in the cytoplasm is  
333 set to maximize the rates of important biochemical reactions. We found that in cycling *Xenopus*

334 egg extracts, the rate of translation, as measured by the synthesis of eGFP from an exogenous  
335 mRNA and the incorporation of  $^{35}\text{S}$ -methionine into endogenous translation products, does peak  
336 at a 1x cytoplasmic concentration, consistent with the maximal speed hypothesis (Figure 2). This  
337 finding fits well with previous studies of cost minimization and near-optimal resource allocations  
338 in models of *E. coli* protein synthesis (Hu et al., 2020; Klumpp et al., 2013; Scott et al., 2014).  
339 However, protein degradation, as measured by DQ-BSA dequenching and CFP-securin  
340 degradation peaks at a higher cytoplasmic concentration,  $\sim 1.8\text{x}$  (Figure 3). The difference in  
341 concentration optima can be explained by the differences in the sensitivities of translation vs.  
342 degradation to viscosity: the viscogen Ficoll 70 is more potent in inhibiting translation than  
343 degradation (Figure 4H, I). This in turn may be due to differences in the sizes of the  
344 macromolecular complexes involved in the two processes, as the diffusion coefficients for large  
345 fluorescent beads are more affected by cytoplasmic concentration than those of smaller beads  
346 (Figure 4E, F). Other factors that might make translation be more diffusion-limited than protein  
347 degradation could also contribute the differential sensitivity of the two processes to changes in  
348 cytoplasmic concentration. The different optimal cytoplasmic concentrations for translation vs.  
349 degradation mean that the system is homeostatic: increasing the concentration of  
350 macromolecules in the cytoplasm would increase the rate of degradation and decreases the rate  
351 of translation, whereas decreasing the cytoplasmic concentration would decrease the rate of  
352 degradation (Figure 5). This behavior can be explained through a theoretical treatment based on  
353 mass action kinetics and Phillip's law (Phillips, 1986; Phillips, 1988).

354 Both the mRNA translation and protein degradation rates measured here were found to smoothly  
355 vary with cytoplasmic concentration (Figures 2 and 3). Thus, there was no evidence for critical  
356 concentrations above or below which the processes abruptly ceased. We suspect that any such  
357 critical points lie outside the range of concentrations examined here. Likewise, the effects of high  
358 cytoplasmic concentration on translation and degradation dynamics appeared to be largely  
359 reversible, since the activities measured in a 2x extract diluted back to 1x were very similar to  
360 those in the original 1x extract (Figures 2 and 3).

361 Although the conventional wisdom is that almost all biochemical reactions are reaction-  
362 controlled (i.e., the catalytic rate constant  $k_2$  is much smaller than  $k_{-1}$ ) rather than diffusion  
363 controlled ( $k_{-1}$  is much smaller than  $k_2$ ) (Bar-Even et al., 2011; Davidi et al., 2016), both of the

364 processes measured here were inhibited by the crowding agent/viscogen Ficoll 70, with  
365 translation substantially more sensitive than degradation. The simplest interpretation is that  
366 translation (in particular) is running relatively close to the diffusion limit, possibly because in the  
367 extract, the diffusion of large macromolecules required for dissociation ( $k_{-1}$ ) is quite slow.

368 Note that the shapes of the rate curves mean that protein synthesis and degradation can be  
369 viewed as a negative feedback system. Increasing the cytoplasmic protein concentration  
370 increases the cytoplasmic viscosity, which negatively affects translation, which makes the  
371 protein concentration eventually drop—a negative feedback loop based on the sensitivity of  
372 translation to viscosity. Conversely, decreasing the cytoplasmic protein concentration decreases  
373 the cytoplasmic viscosity, which mitigates the drop in translation rates that would normal be  
374 expected from a decrease in ribosome and mRNA concentration. Such feedback regulation may  
375 also pertain to the oscillation of biomass growth rate and maintenance of cytoplasmic density  
376 found in single mammalian cells (Liu et al., 2020). Negative feedback is a common theme in  
377 homeostatic systems. This process can alternatively be viewed as a variation on end product  
378 inhibition, where the product of protein synthesis inhibits translation, but through the  
379 intermediacy of changes in protein diffusion rates rather than through the direct binding of the  
380 product to the enzyme.

381 We do not yet have direct evidence for the time scale of this proposed protein concentration  
382 homeostasis. Based on the measurement of 43 h for the median half-life of a *Xenopus* protein  
383 during embryogenesis (Peshkin et al., 2015), we suspect that the response might require tens of  
384 hours. This time scale would be particularly appropriate for protein homeostasis in the immature  
385 oocyte, the egg's immediate precursor in development. The oocyte is thought to live for weeks or  
386 months in the frog ovary and to vary little in terms of size, appearance, and composition during  
387 this time (Ferrell, 1999; Smith et al., 1991). In contrast, the changes in protein synthesis and  
388 degradation are likely to be too slow make a significant impact during the decrease in  
389 cytoplasmic concentration that occurs during mitosis, since embryonic mitosis is only about 15  
390 min in duration.

### 391 **Acknowledgements**

392 This work was supported by a grant from the NIH (R35 GM131792) to J.E.F.

393 **Author contributions**

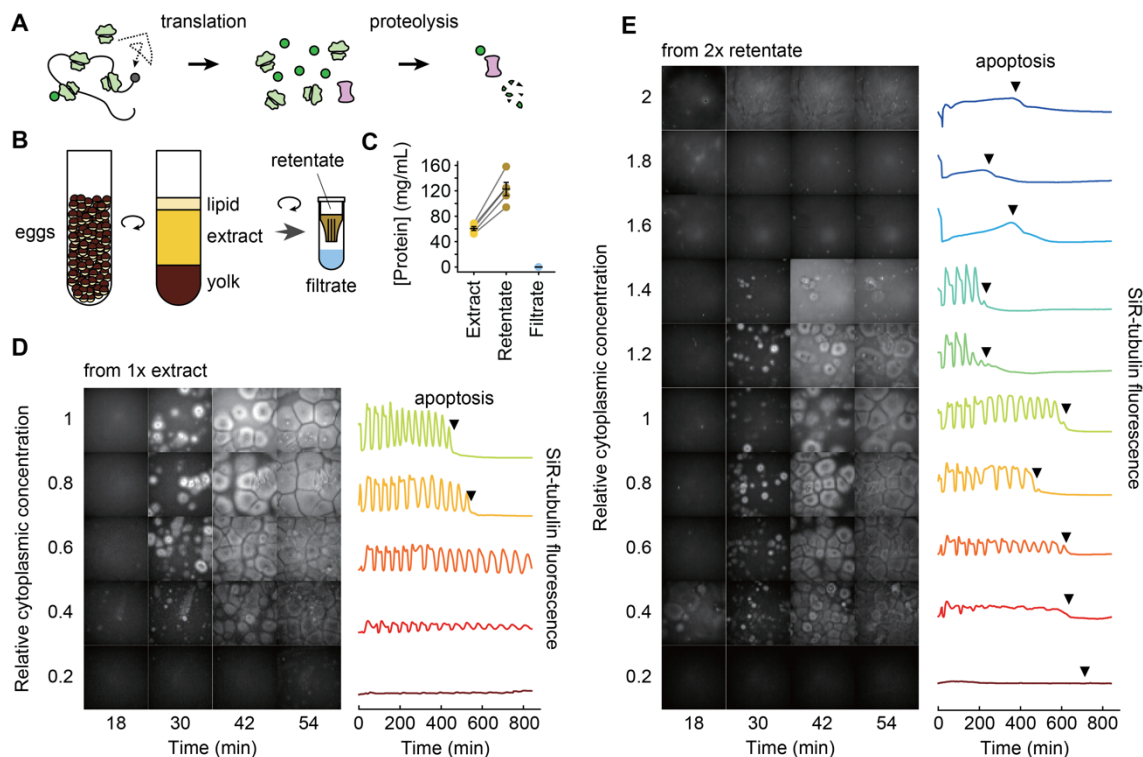
394 Conceptualization, Y.C., J.H., and J.E.F.; Methodology, Y.C., J.H, C.P., and J.E.F.; Software,  
395 Y.C.; Formal Analysis, Y.C. and J.E.F.; Investigation, Y.C.; Resources, C.P.; Writing – Original  
396 Draft, Y.C. and J.E.F.; Visualization, Y.C. and J.E.F.; Supervision, J.E.F.; Funding Acquisition,  
397 J.E.F.

398 **Declaration of interests**

399 The authors declare no competing interests.

400

401



402

403 **Figure 1. General properties of diluted and concentrated *Xenopus* egg extracts: effects on**  
404 **self-organization and cycling**

405 (A) Schematic view of protein synthesis and degradation.

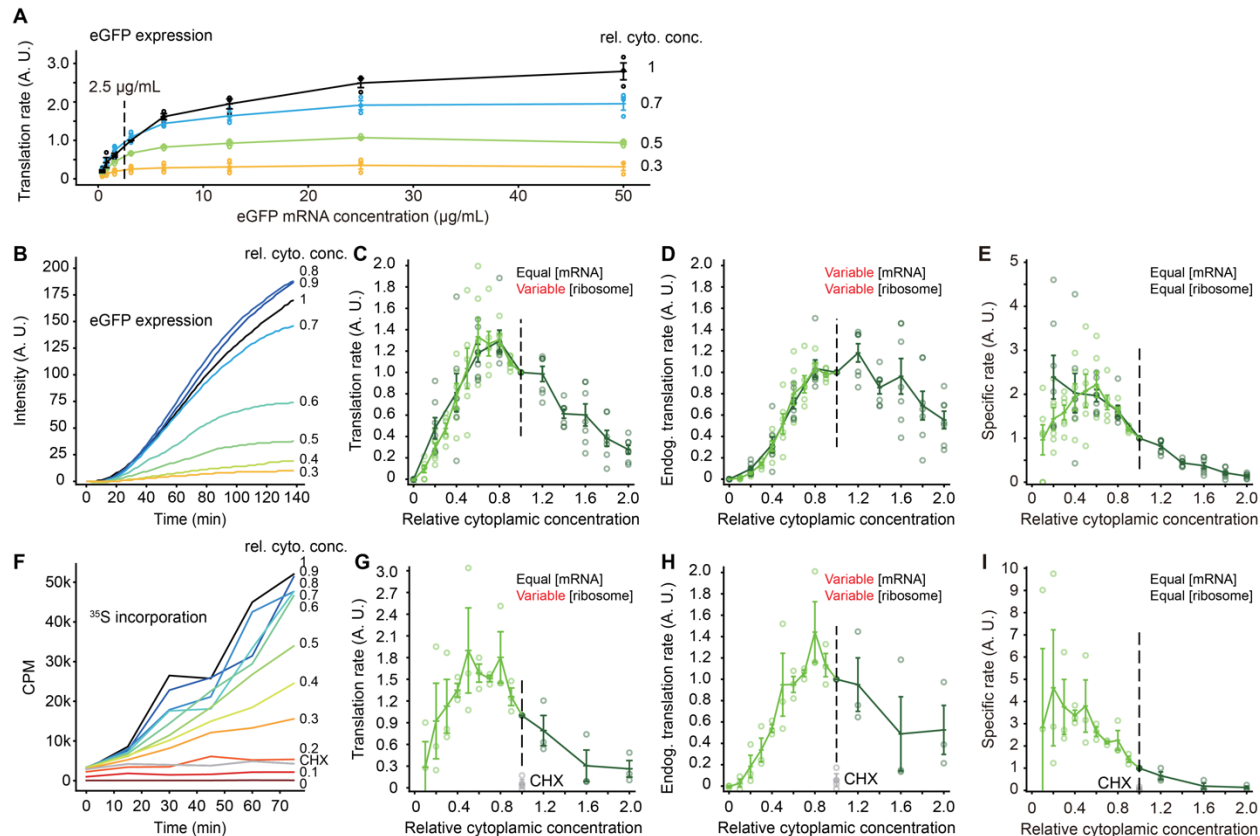
406 (B) Preparation of *Xenopus* egg extract, 2x concentrated retentate, and protein-depleted filtrate.

407 (C) Protein concentration in extract, retentate, and filtrate. Concentrations were determined by  
408 Bradford assays. Data are from five extracts. Individual data points are overlaid with the means  
409 and standard errors.

410 (D) SiR-tubulin staining (left) and SiR-tubulin fluorescence intensity as a function of time (right)  
411 in an extract after various dilutions. The starting material was a 1x extract, diluted with various  
412 proportions of filtrate and imaged in a 96-well plate under mineral oil. All fields are shown at  
413 equal exposure. The fluorescence intensities shown on the right were quantified from the center  
414 1/9 of the wells.

415 (E) SiR-tubulin staining (left) and SiR-tubulin fluorescence intensity as a function of time (right)  
416 in an extract after various dilutions. The data were collected as in (D) except that the starting  
417 material was a 2x extract.

418



419

420 **Figure 2. The rate of mRNA translation is maximal at a cytoplasmic concentration of ~1x.**

421 (A) Titration of mRNA concentration for eGFP expression. The indicated concentration (2.5  
422 μg/mL) was chosen for the experiments in (B-E).

423 (B) eGFP expression as a function of time for various dilutions of a 1x extract.

424 (C) Translation rate as a function of cytoplasmic concentration. These are the directly-measured  
425 data from experiments where the eGFP mRNA concentration was kept constant and the  
426 translation machinery was proportional to the cytoplasmic concentration. Data are from 6  
427 experiments for dilution from 1x extracts and 7 experiments for dilution from 2x retentates. Data  
428 are normalized relative to the translation rates at a cytoplasmic concentration of 1x. Means and  
429 standard errors are overlaid on the individual data points. In this and the subsequent panels, the  
430 darker green represents data from diluting 2x retentates and the lighter green from diluting 1x  
431 extract.

432 (D) Inferred translation rates for the situation where the mRNA concentration as well as the  
433 ribosome concentration is proportional to the cytoplasmic concentration. The rates from (C) were  
434 multiplied by the relative cytoplasmic concentrations.

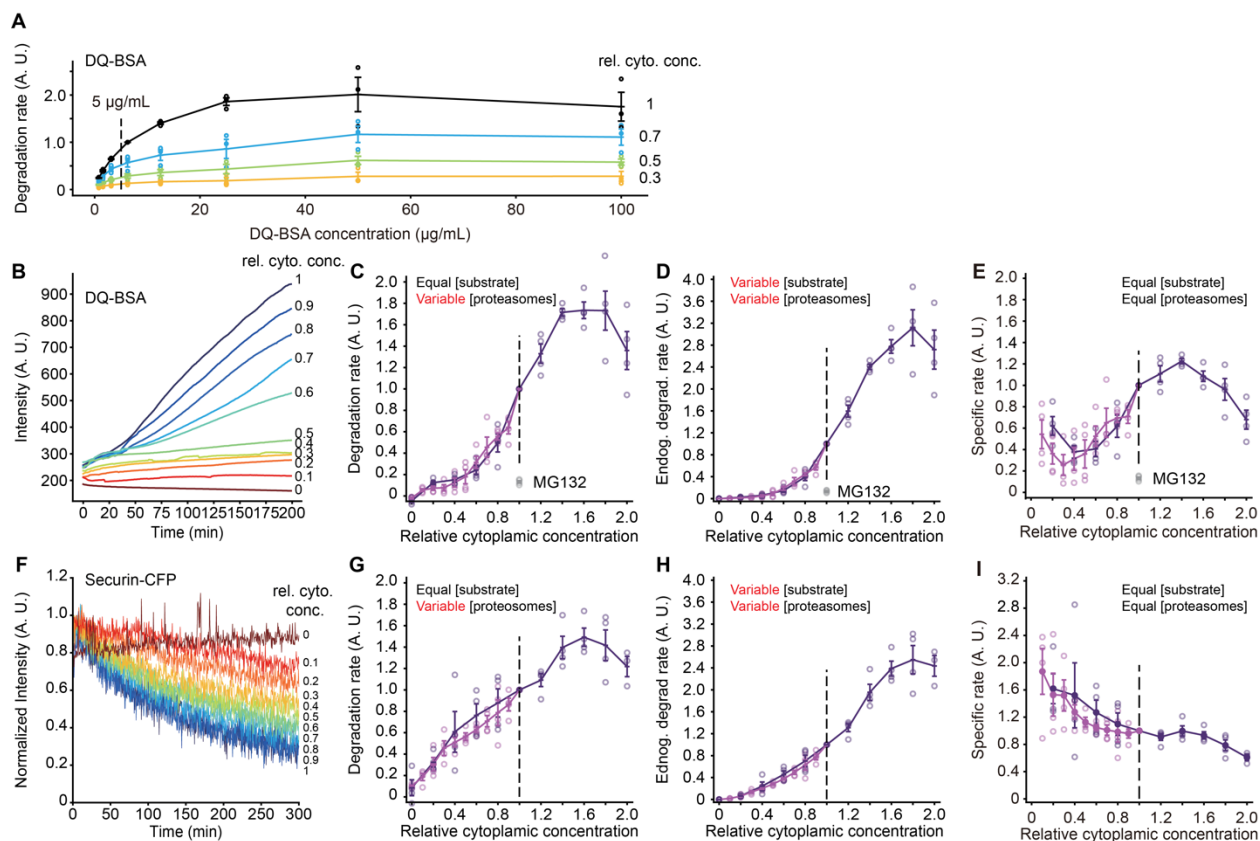
435 (E) Inferred translation rates for the situation where both the mRNA concentration and the  
436 ribosome concentration are kept constant at all dilutions. The rates from (C) were divided by the  
437 relative cytoplasmic concentrations.

438 (F) TCA-precipitable  $^{35}\text{S}$  incorporation as a function of time for translation from endogenous  
439 mRNAs. Various dilutions of a 1x extract are shown. CHX denotes a 1x extract treated with 100  
440  $\mu\text{g}/\text{mL}$  cycloheximide.

441 (G) Inferred translation rates for the situation where mRNA concentration is kept constant and  
442 ribosome concentration is proportional to the cytoplasmic concentration. The rates from (H)  
443 were divided by the relative cytoplasmic concentration. The grey data points are from CHX (100  
444  $\mu\text{g}/\text{mL}$ )-treated 1x extracts.

445 (H) Translation rate as a function of cytoplasmic concentration. These are the directly-measured  
446 data from experiments where the  $^{35}\text{S}$  concentration was kept constant but both the (endogenous)  
447 mRNA concentration and translational machinery were proportional to the cytoplasmic  
448 concentration. Data are from 3 experiments for dilution from 1x extracts and 3 experiments for  
449 dilution from 2x retentates. Data are normalized relative to the translation rates at a cytoplasmic  
450 concentration of 1x. Means and standard errors are overlaid on the individual data points.

451 (I) Inferred translation rates for the situation where both the mRNA concentration and the  
452 ribosome concentration are kept constant at all dilutions. The rates from (H) were divided twice  
453 by the relative cytoplasmic concentrations (i.e. by the relative concentration squared).



454

455 **Figure 3. The rate of protein degradation is maximal at cytoplasmic concentrations of**  
456 **~1.8x.**

457 (A) Titration of substrate protein concentration for DQ-BSA degradation experiments. The  
458 indicated concentration (5 µg/mL) was chosen for the experiments in (B-E).

459 (B) DQ-BSA fluorescence as a function of time for various dilutions of a 1x extract.

460 (C) Degradation rate as a function of cytoplasmic concentration. These are the directly-measured  
461 data from experiments where the DQ-BSA concentration was kept constant and the proteolysis  
462 machinery was proportional to the cytoplasmic concentration. The grey data points denoted  
463 MG132 are from 1x extracts treated with 200 µM MG132, a proteasome inhibitor. Data are from  
464 4 experiments for dilution from 1x extracts and 4 experiments for dilution from 2x retentates.

465 Data are normalized relative to the degradation rates at a cytoplasmic concentration of 1x. Means  
466 and standard errors are overlaid on the individual data points. In this and the subsequent panels,  
467 the darker purple represents data from diluting 2x retentates and the lighter purple from diluting  
468 1x extract.

469

470 (D) Inferred degradation rates for the situation where the substrate concentration as well as the  
471 proteasome concentration is proportional to the cytoplasmic concentration. The rates from (C)  
472 were multiplied by the relative cytoplasmic concentrations.

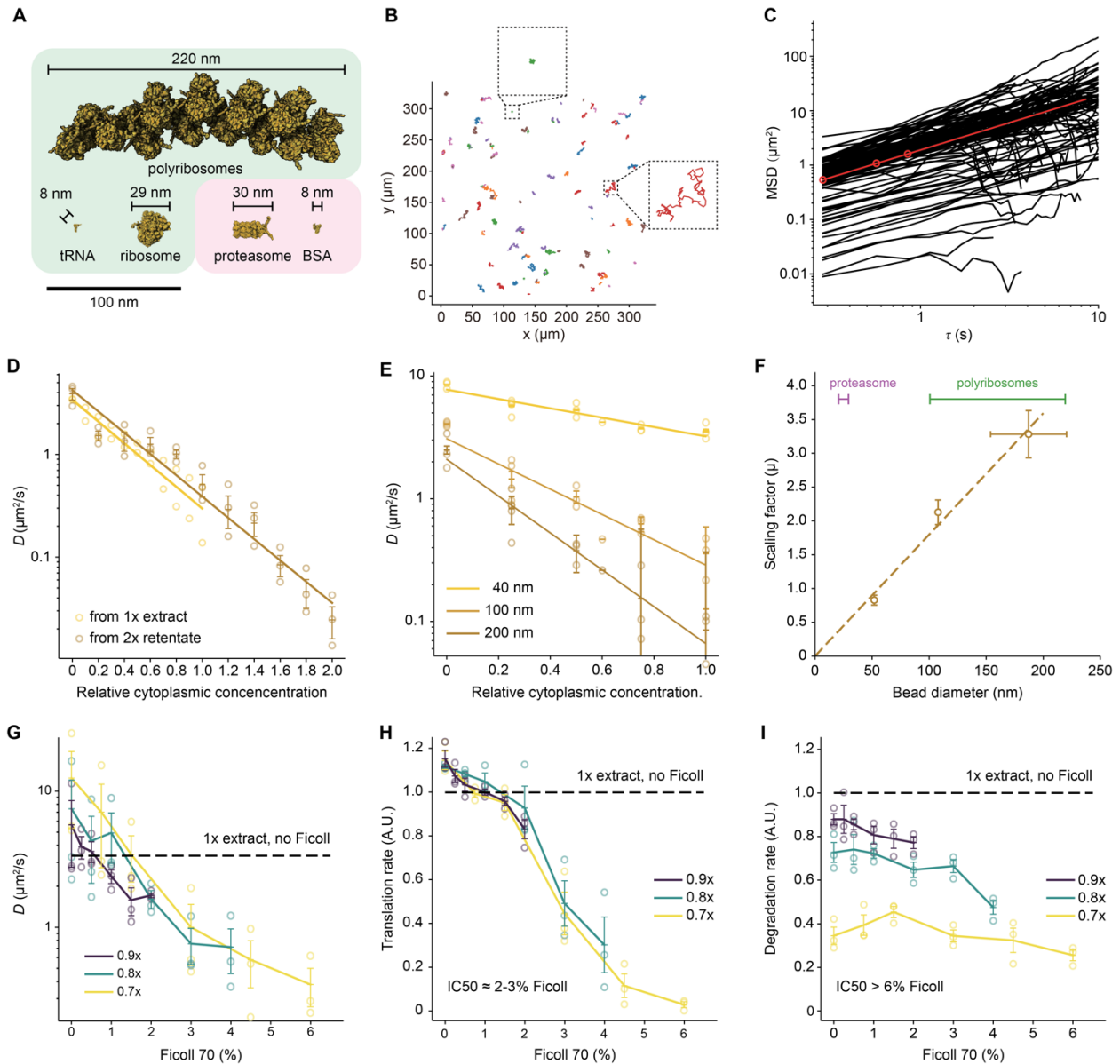
473 (E) Inferred degradation rates for the situation where both the substrate concentration and the  
474 proteasome concentration are kept constant at all dilutions. The rates from (C) were divided by  
475 the relative cytoplasmic concentrations.

476 (F) Degradation of securin-CFP as a function of time for various dilutions of a 1x extract.

477 (G) Degradation rate as a function of cytoplasmic concentration. These are the directly-measured  
478 data from experiments where the securin-CFP concentration was kept constant but the  
479 proteasome concentration was proportional to the cytoplasmic concentration. Data are from 4  
480 experiments for dilution from 1x extracts and 4 experiments for dilution from 2x retentates. Data  
481 are normalized relative to the degradation rates at a cytoplasmic concentration of 1x. Means and  
482 standard errors are overlaid on the individual data points.

483 (H) Inferred degradation rate for the situation where both the substrate and proteasome  
484 concentrations are proportional to the cytoplasmic concentration. The rates from (G) were  
485 multiplied by the relative cytoplasmic concentrations.

486 (I) Inferred degradation rates for the situation where both the substrate and the proteasome  
487 concentration are kept constant at all dilutions. The rates from (G) were divided by the relative  
488 cytoplasmic concentrations.



489

490 **Figure 4. The effect of cytoplasmic concentration on diffusion, and the effect of Ficoll 70 on**  
 491 **translation and protein degradation.**

492 (A) The sizes of various macromolecules and complexes involved in translation and degradation.

493 (B) Single particle traces for diffusion of 100 nm fluorescent beads in 1x cytoplasmic extracts.

494 Two examples of location-to-location variability are highlighted.

495 (C) Mean-squared displacement for 110 individual trajectories (black) and average mean-squared

496 displacement (red) as a function of the time difference  $\tau$ . Effective diffusion coefficients were

497 calculated from the first 1 s of data.

498 (D) Effective diffusion coefficients for 100 nm fluorescent beads as function of relative  
499 cytoplasmic concentration. Data are from 3 experiments for the 2x extract dilution and from 2  
500 experiments for the 1x extract dilution. Error bars for the 2x extract dilution represent means  $\pm$   
501 standards errors.

502 (E) Effective diffusion coefficients for beads of different diameter (nominally 40 nm, 100 nm,  
503 and 200 nm) as a function of relative cytoplasmic concentration. Data are from 3 experiments.  
504 Means and standard errors are overlaid on the individual data points.

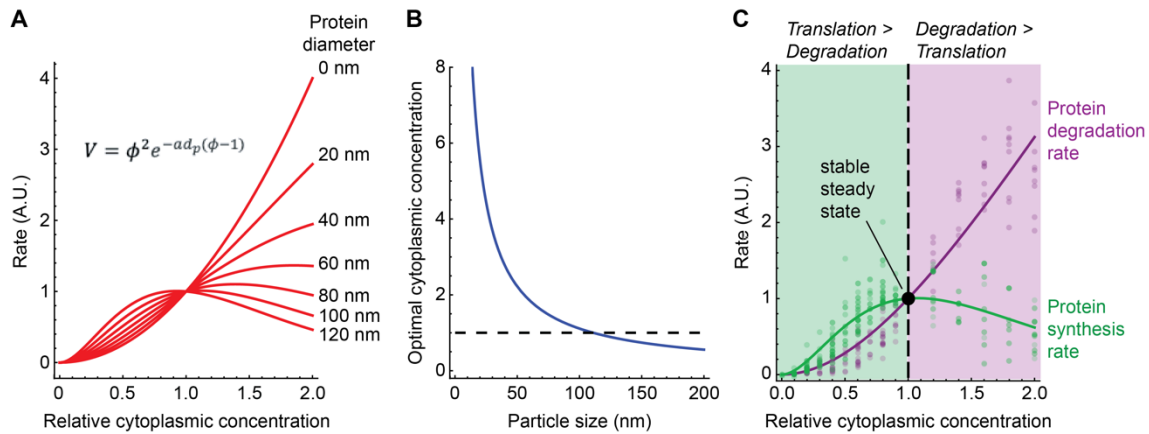
505 (F) The scaling factor  $\mu$  (from Eq. 1) as a function of bead diameter. The apparent bead  
506 diameters (nominally 40, 100, and 200 nm) were calculated from their diffusion coefficients in  
507 extract buffer with no sucrose using the Stokes-Einstein relationship. Scaling factors are from 3  
508 experiments and are shown as means  $\pm$  S.E. Bead diameters are from 3 experiments for the 40  
509 nm beads and 4 experiments for the 100 and 200 nm beads, and again are plotted as means  $\pm$  S.E.  
510 The diameters of proteosomes and polyribosomes are shown for comparison.

511 (G) Diffusion coefficients of 40 nm beads as a function of Ficoll 70 concentration. Extracts were  
512 prepared at 0.7x, 0.8x, and 0.9x as indicated and supplemented with Ficoll to yield the final  
513 concentrations (w/vol) shown on the  $x$ -axis. Data are from 3 experiments. Means and standard  
514 errors are overlaid on the individual data points. Diffusion coefficients for the undiluted 1x  
515 extracts were also measured and the average is shown for reference.

516 (H) Translation rates, using the eGFP assay, as a function of Ficoll 70 concentration. Extracts  
517 were prepared at 0.7x, 0.8x, and 0.9x as indicated and supplemented with Ficoll to yield the final  
518 concentrations (w/vol) shown on the  $x$ -axis. Data are from the same 3 experiments shown in (G).  
519 Means and standard errors are overlaid on the individual data points. Translation rates for the  
520 undiluted 1x extracts were also measured and the average is shown for reference.

521 (I) Degradation rates, using the DQ-BSA assay, as a function of Ficoll 70 concentration. Extracts  
522 were prepared at 0.7x, 0.8x, and 0.9x as indicated and supplemented with Ficoll to yield the final  
523 concentrations (w/vol) shown on the  $x$ -axis. Data are from the same 3 experiments shown in (G).  
524 Means and standard errors are overlaid on the individual data points. Degradation rates for the  
525 undiluted 1x extracts were also measured and the average is shown for reference.

526



527

528 **Figure 5. Homeostasis in a model of the effect of cytoplasmic concentration of translation**  
529 **and protein degradation.**

530 (A) Plot of Eq. 11, which relates a bimolecular reaction rate to the relative cytoplasmic  
531 concentration, for various sizes of proteins. We assumed  $a = 0.018 \text{ nm}^{-1}$  (from Figure 4F).

532 (B) Calculated optimal relative cytoplasmic concentration for proteins of different assumed sizes,  
533 again assuming  $a = 0.018 \text{ nm}^{-1}$

534 (C) Fits of Eq. 11 to the experimental data for translation (green) and degradation (purple) as a  
535 function of cytoplasmic concentration, calculated assuming that both the substrate and enzyme  
536 varied with the cytoplasmic concentration. All of the data from Figures 2D, H and 3D, H were  
537 included in the fits. The  $R^2$  values are 0.92 for the translation data and 0.95 for the degradation  
538 data. The fitted values for the size of the proteins involved are  $104 \pm 2 \text{ nm}$  (mean  $\pm$  S.E.) for  
539 translation and  $14 \pm 1 \text{ nm}$  (mean  $\pm$  S.E) for degradation. The fitted optimal cytoplasmic  
540 concentrations are  $1.07 \pm 0.02$  for translation and  $8.1 \pm 0.8$  for degradation (mean  $\pm$  S.E.).

541

## 542 **Star Methods**

### 543 **Extract preparation**

544 Cycling extracts were prepared as described previously (Chang and Ferrell, 2018; Murray, 1991)  
545 with the following modifications. Briefly, freshly laid frog eggs were collected, washed with 20  
546 g/L L-cysteine pH 7.8, and incubated for 3-5 min to remove the jelly coat. The eggs were then  
547 washed twice with ~150 mL 0.2x 6s (MMR) solution (20 mM NaCl, 1 mM HEPES, 400  $\mu$ M  
548 KCl, 400  $\mu$ M CaCl<sub>2</sub>, 200  $\mu$ M MgCl<sub>2</sub>, and 20  $\mu$ M EDTA pH 7.8) and resuspended in 50 mL 0.2x  
549 MMR solution. Calcium ionophore A23187 (C7522, Sigma) was added to a final concentration  
550 of 0.5  $\mu$ g/mL to activate the eggs. After 2 min of activation, liquid was removed, and the eggs  
551 were washed twice with ~150 mL 0.2xMMR solution and three times with ~150 mL extract  
552 buffer [100 mM KCl, 50 mM sucrose, 10 mM HEPES pH 7.7 (with KOH), 1 mM MgCl<sub>2</sub>, and  
553 100  $\mu$ M CaCl<sub>2</sub>]. Twenty min after activation (>80% of the eggs showed contraction of the  
554 animal pole), the eggs were transferred to a 14 mL round-bottom polypropylene tube (352059,  
555 Corning) and packed for 1 min at 300  $\times$  g. Excess liquid on top of the eggs was removed, and the  
556 egg-containing tube was chilled on ice. The eggs were crushed by centrifugation at 16,000  $\times$  g  
557 for 15 min at 4°C. The cytoplasmic layer was then collected by puncturing the side of the  
558 extract-containing tube at ~2 mm above the interphase between the extract layer and the yolk  
559 layer. The extract was allowed to flow into a collecting Eppendorf tube by gravity or by gently  
560 pressing the tube opening with one finger to create a positive pressure inside the tube. The  
561 collected extract was mixed with 10  $\mu$ g/mL leupeptin, 10  $\mu$ g/mL pepstatin, 10  $\mu$ g/mL  
562 chymostatin, and 10  $\mu$ g/mL cytochalasin B, and further refined by centrifugation at 16,000  $\times$  g  
563 for 5 min at 4°C using a tabletop refrigerated centrifuge. After the refining centrifugation, the  
564 clarified extract was transferred to a new tube.

565 CSF extracts (Kamenz et al., 2021; Murray, 1991) were prepared similarly to cycling extracts,  
566 with the differences being that the eggs were washed with ~150 mL CSF extract buffer (100 mM  
567 KCl, 50 mM sucrose, 10 mM potassium HEPES pH 7.7, 5 mM EGTA pH 7.7, 2 mM MgCl<sub>2</sub>, and  
568 0.1 mM CaCl<sub>2</sub>) four times immediately after dejellied, without 0.2x MMR washes or calcium  
569 ionophore activation. The whole process between dejellying and the crushing spin typically took  
570 ~10 min. After the refining centrifugation, the extract was transferred to a new tube and  
571 supplemented with 100  $\mu$ g/mL cycloheximide.

## 572 **Filtrate and retentate preparation**

573 Extract (400  $\mu\text{L}$ ) was transferred to a 10 kDa molecular weight cut-off centrifugal filter unit  
574 (UFC501096, Millipore) placed in a collection tube and centrifuged at  $16,000 \times g$  for 10 min at  
575  $4^\circ\text{C}$  three times. After each centrifugation period, the extract was taken out of the centrifuge and  
576 mixed by pipetting. The filtrate was collected in the collection tube, and the retentate was  
577 collected from the filtration unit.

## 578 **SiR-tubulin intensity**

579 To monitor microtubules in cycling extracts, 200 nM SiR-tubulin was added to the extract,  
580 retentate, and filtrate. Then the extract or retentate was mixed with different volume fractions of  
581 filtrate to create a series of dilution conditions. Five  $\mu\text{L}$  of the dilutions were loaded onto a 96  
582 well polystyrene assay plate (3368, Corning) and gently spread using the pointed end of the  
583 loading pipette tip to allow even coverage of extract at the bottom of the well. A layer of 100  $\mu\text{L}$   
584 heavy mineral oil (330760, Sigma) was pipetted to cover the extract and prevent evaporation.  
585 The 96 well plate was immediately loaded onto an inverted epi-fluorescence microscope (DMI8,  
586 Leica) for imaging at a frame rate of  $0.5 \text{ min}^{-1}$ . The median intensity from the center 1/9 of each  
587 frame was measured and plotted with off-sets in Figures 1D and 1E.

## 588 **eGFP translation and DQ-BSA degradation**

589 For eGFP translation and DQ-BSA degradation experiments, the extract, filtrate, or retentate was  
590 mixed with 2.5 ng/ $\mu\text{L}$  (unless otherwise stated) eGFP mRNA (L-7201-100, Trilink  
591 Biotechnologies) or 5 ng/ $\mu\text{L}$  DQ-BSA (D12050, Thermo Fisher) on ice. The extract or retentate  
592 was mixed with different proportions of the filtrate to generate different dilutions. The dilutions  
593 (15  $\mu\text{L}$ ) were then added to a clear bottom 384-well plate (324021, Southern Labware) and  
594 equilibrated to room temperature. The imaging plate was then loaded onto an inverted  
595 fluorescence microscope for time course measurements at a frame rate of  $1 \text{ min}^{-1}$  or  $0.5 \text{ min}^{-1}$ .

596 To calculate the rate of eGFP protein synthesis and DQ-BSA degradation, the median intensity  
597 of the center quarter of each frame was measured. The raw rates were extracted by calculating  
598 the slope of a linear segment from the intensity-time plot. The linear segment was typically  
599 between 50 and 120 min for eGFP translation, and between 25 and 120 min for DQ-BSA  
600 degradation experiments. Intensity trajectories were manually inspected and the linear segments

601 were adjusted individually to ensure linearity. The raw rates from dilutions of 1x extract (or 2x  
602 retentate) were normalized by the rate measured in the original 1x extract (or the reconstituted 1x  
603 extract) from the same batch of eggs to control for variability due to batch variation of the eggs  
604 and experimental conditions, allowing comparison among experiments.

#### 605 **<sup>35</sup>S-methionine labeling**

606 A cycling extract was concentrated as described above. The extract, retentate, and filtrate were  
607 supplemented with 1% v/v <sup>35</sup>S-methionine to a final concentration of ~0.5 μCi/μL. The filtrate  
608 was then mixed with different volume fractions of extract or retentate to generate a series of  
609 dilutions. For the “CHX” sample, 100 μg/mL cycloheximide was added to a 1x extract. The  
610 extract was then sampled at 15-min intervals, and the translation process was halted by directly  
611 mixing 5 μL samples with 100 μL H<sub>2</sub>O, which was then mixed with 100 μL 50% TCA  
612 (trichloroacetic acid, T0699, Sigma). To collect and clean up the TCA precipitable material, 50  
613 μL of the homogeneous extract/TCA mixture was passed through a glass fiber filter  
614 (WHA1820025, Sigma) prewetted with 5% TCA, then 1 mL of 5% TCA was passed through the  
615 filter to remove soluble material, and the filter was washed with 2 mL of 95% ethanol and dried  
616 on vacuum. The filter with collected material was dropped into a 20-mL scintillation vial (03-  
617 337-2, Thermo Fisher) containing 10 mL scintillation fluid (111195, RPI Research Products).  
618 The radioactivity was measured using a liquid scintillation counter. The rate was calculated  
619 similarly to the eGFP translation and DQ-BSA degradation experiments.

#### 620 **Securin-CFP degradation**

621 The securin-CFP degradation experiments followed a previous protocol (Kamenz et al., 2021)  
622 with modifications. The fluorescent probe, securin-CFP, was made by mixing 10 μg of an SP6-  
623 securin-CFP plasmid in 20 μL H<sub>2</sub>O with 30 μL SP6 High-Yield Wheat Germ Protein Expression  
624 System (TnT® L3261, Promega), and incubating at room temperature for 2 h per the  
625 manufacturer’s instructions. CSF extracts were used for these experiments. The CSF extract was  
626 additionally supplemented with purified recombinant nondegradable Δ90 sea urchin cyclin B  
627 protein at a concentration capable of driving the extract into an M-phase arrest and incubated at  
628 room temperature for 30 min. 0.8 mM CaCl<sub>2</sub> was added to the extract and incubated for an  
629 additional 30 min to degrade endogenous cyclin B. The extract was then divided into two

630 fractions, one kept on ice and the other concentrated using the previously stated method. A series  
631 of dilutions were reconstituted by mixing the filtrate with either the extract kept on ice or  
632 retentate from the concentrator. 19  $\mu\text{L}$  of the extracts were added and mixed with 1  $\mu\text{L}$  of the in  
633 vitro transcribed and translated securin-CFP and pipette into a glass-bottomed 384-well plate. As  
634 a background control, we also included a well of extract with no securin-CFP. The time courses  
635 of fluorescence intensity were recorded using a fluorescence plate reader at a rate of  $2 \text{ min}^{-1}$ .

636 To calculate the degradation rate, each experimental reading was subtracted by the  
637 corresponding background measurement. The first few data points typically increased with time,  
638 possibly due to equilibration of the fluorophore. Therefore, instead of normalizing to the first  
639 data point in each time series, the background corrected intensities were divided by the  
640 maximum of the first 15 time points (7.5 min). The normalized intensities were fitted to  $A = A[0]$   
641  $e^{-kt} + C$ , where  $A$  is the fluorescence,  $k$  is the rate constant, and  $t$  is time, and  $A[0]$  (constrained to  
642 be greater than 0.95),  $k$ , and  $C$  (constrained between 0 and 0.05) are fitting variables. The value  
643 of  $k$  measured for each dilution condition from 1x extract (or from 2x retentate) was normalized  
644 to 1x extract (or nominal 1x reconstituted from the 2x retentate) from the same experiment to  
645 control for variations among batches of eggs.

### 646 **Single particle tracking**

647 PEGylated fluorescent particles were prepared by mixing 50  $\mu\text{L}$  of 20 mg/mL  
648 methoxypolyethylene glycol amine 750 (07964, Sigma), 5  $\mu\text{L}$  of fluorescent polystyrene nano  
649 beads (2% solid, F8888 and F8795, Thermo Fisher), 50  $\mu\text{L}$  of 30 mM N-  
650 hydroxysulfosuccinimide (56485, Sigma) in 200 mM borate buffer pH8.2, and 10  $\mu\text{L}$  of 100 mM  
651 N-(3-dimethylaminopropyl)-N'-ethylcarbodiimide hydrochloride (03450, Sigma). The  
652 PEGylation reaction was incubated at room temperature for 20 h. The reaction was then stopped  
653 by 1:100 dilution with water, dialysis with 3 M NaCl, and three subsequent dialyses with water.  
654 The particles were diluted further to make it so that a 1:100 dilution provided a suitable  
655 concentration for segmentation and tracking. 1:100 (v:v) of the beads were mixed into the extract  
656 by pipetting. 5  $\mu\text{L}$  of the extract was placed in the center of a well in a glass-bottom 96-well  
657 plate. The plate was loaded onto an inverted epifluorescence microscope. The extract was  
658 allowed to equilibrate with the environment for 5 min, and a movie was taken at the appropriate  
659 wavelength at a frame rate of 3 Hz using a 40x objective.

660 The time-lapse videos of particle movements were analyzed with a custom Python script.  
661 Briefly, the images were flat field corrected (background flat fields were generated using BaSiC,  
662 an ImageJ package) and bleach corrected. The particles were called and linked using the Trackpy  
663 library with adaptive mode, which allows calling particle movements with large step size  
664 variations. Typical starting parameters for Trackpy were: diameter = 15, maxsize = 7, minmass =  
665 650, search\_range = 30, ecc\_threshold = 1, percentile = 99.5, topn = 300, memory = 1; drift  
666 correction was typically off unless the movie had a translational flow. Movies were discarded if  
667 they contained a strong convergent or divergent flow. Parameters were adjusted for individual  
668 movies to allow capturing the greatest number of tracks without sacrificing tracking quality. The  
669 mean squared displacement for an individual trajectory was calculated by  $\langle n\Delta t \rangle =$   
670  $\frac{1}{N-n-1} \sum_{i=1}^{N-n-1} [x(i\Delta t + n\Delta t) - x(i\Delta t)]^2 + [y(i\Delta t + n\Delta t) - y(i\Delta t)]^2$ , where  $N$  is the number  
671 of frames in a trajectory and  $x$  and  $y$  are the coordinates at  $i\Delta t$  or  $i\Delta t + n\Delta t$ . The ensemble mean  
672 squared displacement was calculated by  $\langle n\Delta t \rangle = \sum_{i=1}^K (N_i - n - 1) MSD_i(n\Delta t)$ , where  $K$  is the  
673 number of trajectories,  $N_i$  is the number of frames for the  $i^{\text{th}}$  trajectory, and  $MSD_i(n\Delta t)$  is the  
674 individual MSD of the  $i^{\text{th}}$  trajectory for a time lag of  $n\Delta t$ .

### 675 **Estimation of the effective diffusion coefficient for the time scale of 1 s**

676 To calculate the effective diffusion coefficient,  $D_{eff}$ , a linear fit was made to the first 3 values to  
677 the ensemble MSD vs  $\tau$  plot (corresponding to  $\tau = 1/3, 2/3, \text{ and } 1\text{ s}$ ). The slope of the fitted line  
678 was calculated to obtain  $MSD/\tau$ . The effective diffusion coefficient was calculated by  $D_{eff} =$   
679  $MSD/(4 \tau)$ .

### 680 **Particle size estimation**

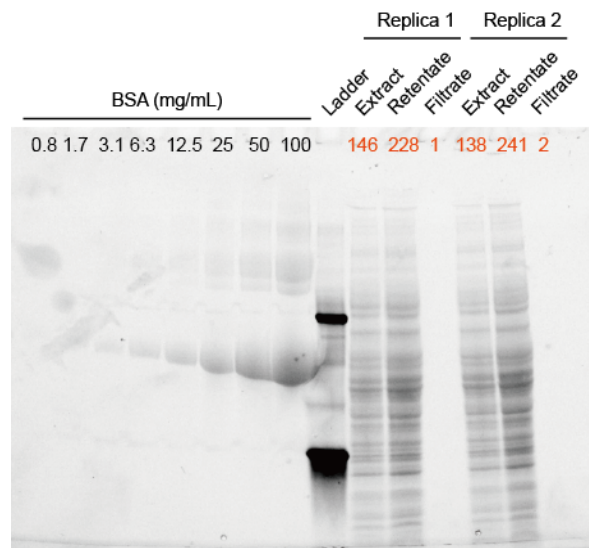
681 PEGylated particles were resuspended in an extract buffer without sucrose. The effective  
682 diffusion coefficient for each type of particle was measured by particle tracking as above. The  
683 diameters of the particles were calculated using a rearrangement of the Stokes-Einstein equation:  
684  $d_{par} = k_B T / (3\pi\eta D_{eff})$ , where  $k_B$  is the Boltzmann constant ( $1.380649 \cdot 10^{-23} \text{ N m K}^{-1}$ ),  $T$  is  
685 temperature (296.15 K), and  $\eta$  is the viscosity of extract buffer without sucrose (assumed to be  
686 similar to water at  $0.001 \text{ N m}^{-2} \text{ s}$ ).

687

688

## Supplementary Information

689

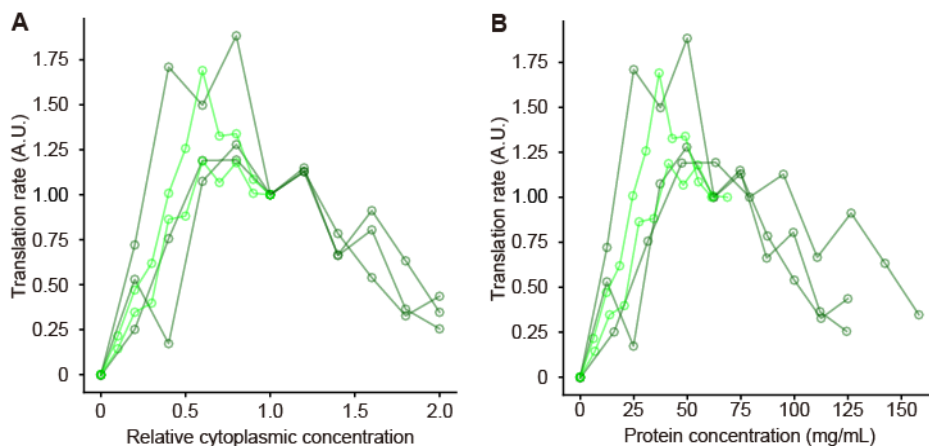


690

691 **Figure S1. Trihalo compound-stained PAGE gel of proteins from 1x extract, filtrate, and 2x**  
692 **retentate**

693 A representative trihalo compound-stained PAGE gel showing a BSA standard and two  
694 biological replicates of extract, retentate, and filtrate. The estimated protein concentrations in  
695 mg/mL (using the BSA standard as a reference) for the extract, retentate, and filtrate samples are  
696 shown in orange. However, it should be noted that the trihalo compound used in staining the gel  
697 depends on tryptophan residues to fluoresce. Since BSA has only 0.3% tryptophan residues  
698 (compared to 1% in proteins overall), the protein concentrations in the extract, retentate, and  
699 filtrate samples are likely overestimated. By Bradford assay the typical protein concentration of  
700 extracts was 50-70 mg/mL.

701



702

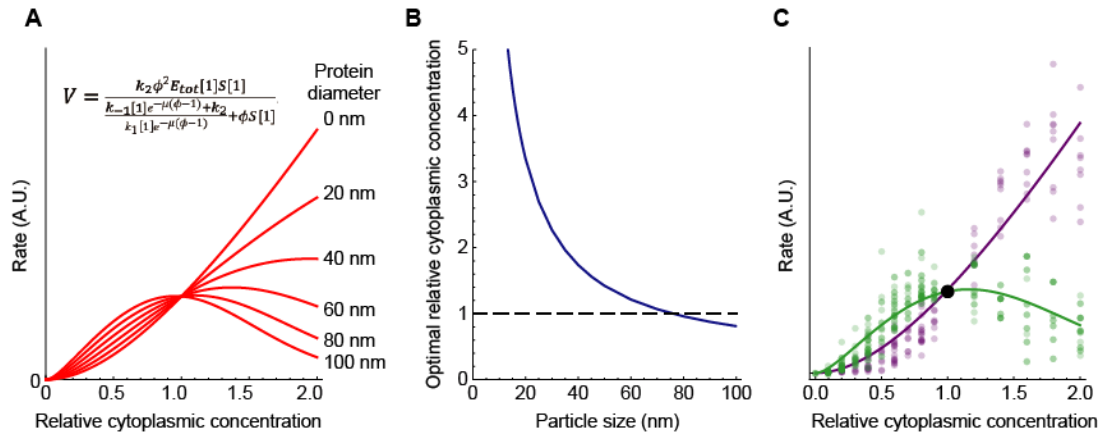
703 **Figure S2. Using nominal vs. measured protein concentrations to compare translation rates**  
704 **in different experiments.**

705 (A) Translation rate as a function of nominal cytoplasmic concentration. These are the directly-  
706 measured data from experiments where the eGFP mRNA concentration was kept constant and  
707 the translation machinery was proportional to the cytoplasmic concentration. Data points from  
708 same experiment are connected. Data are normalized relative to the translation rates at a  
709 cytoplasmic concentration of 1x. Relative cytoplasmic concentration are assumed to be 1.0 for  
710 1x extract and 2.0 for the 2x retentate.

711 (B) Translation rate as a function of measured protein concentration. These are the directly-  
712 measured data from experiments where the eGFP mRNA concentration was kept constant and  
713 the translation machinery was proportional to the cytoplasmic concentration. Data points from  
714 same experiment are connected. Data are normalized relative to the translation rates at a  
715 cytoplasmic concentration of 1x. Protein concentrations were measured for the starting extract  
716 and the retentate, instead of assuming that they were 1x and 2x. Protein concentrations for the  
717 dilutions were calculated from these the respective starting material. Note that the experiment-to-  
718 experiment variation is similar regardless of whether nominal or measured protein concentrations  
719 are used.

720

721



722

723

724 **Figure S3. Homeostasis in a Michaelis-Menten model of the effect of cytoplasmic**  
725 **concentration of translation and protein degradation.**

726 (A) Plot of Eq. S10, which relates a bimolecular reaction rate to the relative cytoplasmic  
727 concentration, for various sizes of proteins, assuming that Michaelis-Menten kinetics are  
728 relevant. We assumed  $a = 0.018 \text{ nm}^{-1}$  (from Figure 4F) and arbitrarily chose the following values  
729 for the parameters:  $E_{tot}[1] = S[1] = k_1[1] = k_{-1}[1] = k_2[1] = 1$ .

730 (B) Calculated optimal relative cytoplasmic concentration for proteins of different assumed sizes,  
731 assuming the same parameters.

732 (C) Fits of Eq. S10 to the experimental data.

733

734

735

736 **Movie S1. Effects of cytoplasmic concentration on self-organization and cycling in dilutions**  
737 **from 1x extract**

738 SiR-tubulin staining (left) and SiR-tubulin fluorescence intensity as a function of time (right) in  
739 an extract after various dilutions. The same data are shown in Figure 1D. The starting material  
740 was a 1x extract, diluted with various proportions of filtrate and imaged in a 96-well plate under  
741 mineral oil. All fields are shown at equal exposure. The fluorescence intensities shown on the  
742 right were quantified from the center 1/9 of the wells and subsequently rescaled using the  
743 maximum and minimum values to enhance the variability in the intensities, particularly in cases  
744 of low cytoplasmic concentration.

745

746 **Movie S2. Effects of cytoplasmic concentration on self-organization and cycling in dilutions**  
747 **from 2x retentate**

748 SiR-tubulin staining (left) and SiR-tubulin fluorescence intensity as a function of time (right) in  
749 an extract after various dilutions. The data were collected as in Movie S1 except that the starting  
750 material was a 2x retentate. The same data are shown in Figure 1E.

751

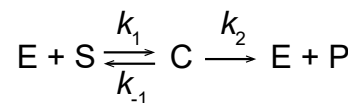
752 **Movie S3. Cell-like compartment formation and cell cycle oscillation in 0.2x and 0.3x**  
753 **cytoplasm**

754 SiR-tubulin staining was conducted on a 0.2x extract (left) and a 0.3x extract (right) as shown in  
755 Movie S1 and Figure 1D. The fluorescence intensities were rescaled to improve the visibility of  
756 the SiR-tubulin staining, and are displayed at a higher magnification,

757 **A model for the effect of diffusion on reaction rates assuming Michaelis-Menten kinetics**

758 In the main text, we derived a simple model to account for the observed rates of protein  
759 translation and degradation as a function of cytosolic protein concentration assuming a mass  
760 action kinetics. Here, we assume a Michaelis-Menten enzymatic reaction kinetics to generate  
761 response curves, and test if such an assumption also accounts the biphasic nature of the response  
762 curves of protein translation and degradation vs cytoplasmic concentration.

763 To start, we assume that the rate determining reaction for each process is a biomolecular  
764 enzymatic reaction:



765

766 where E is the enzyme, S the substrate, C the enzyme-substrate complex, and P the product of  
767 the reaction. If we assume that the system is in steady state, with  $\frac{dC}{dt} = 0$ , and that the substrate  
768 concentration is much higher than the enzyme concentration, then the rate of this process is  
769 described by the Michaelis-Menten equation:

$$V = \frac{dP}{dt} = \frac{k_2 E_{tot} S}{\frac{k_{-1} + k_2}{k_1} + S}, \quad [\text{Eq. S1}]$$

771 where  $E_{tot} = E + C$ .

772 Next we want to add cytoplasmic concentration dependence to the terms on the right-hand side  
773 of Eq. 2. The enzyme and substrate concentrations are linearly proportional to the relative  
774 cytoplasmic concentration  $\phi$ . We can therefore write:

$$E_{tot}[\phi] = \phi E_{tot}[1], \quad [\text{Eq. S2}]$$

$$S[\phi] = \phi S[1]. \quad .[\text{Eq. S3}]$$

777 Substituting into Eq. 2 yields:

$$V = \frac{k_2 \phi^2 E_{tot}[1] S[1]}{\frac{k_{-1} + k_2}{k_1} + \phi S[1]}. \quad [\text{Eq. S4}]$$

778

779 Again, from the Smoluchowski equation (Smoluchowski, 1917) and Phillies's law (Eq. 1)  
780 (Phillies, 1986; Phillies, 1988), we take the diffusion coefficients to be negative exponential  
781 functions of the cytoplasmic protein concentration:

$$782 \quad k_1[\phi] \propto D_E[\phi] + D_S[\phi] = D_E[0]e^{-\mu_E\phi} + D_S[0]e^{-\mu_S\phi}. \quad [\text{Eq. S6}]$$

783 For the special case where either one diffusion coefficient is much smaller than the other, or the  
784 scale factors are equal, we can simplify this to:

$$785 \quad k_1[\phi] = k_1[0]e^{-\mu\phi}. \quad [\text{Eq. S7}]$$

786 Similarly, we can rewrite Eq. S7 as:

$$787 \quad k_1[\phi] = k_1[1]e^{-\mu(\phi-1)}. \quad [\text{Eq. S8}]$$

788 We assume that  $k_{-1}$  varies with the diffusion coefficients and the cytoplasmic concentration in  
789 the same way, and that  $k_2$ , the rate constant for the catalytic step, is independent of the  
790 cytoplasmic concentration. It follows that:

$$791 \quad V = \frac{k_2\phi^2 E_{tot}[1]S[1]}{\frac{k_{-1}[1]e^{-\mu(\phi-1)} + k_2 + \phi S[1]}{k_1[1]e^{-\mu(\phi-1)}}}. \quad [\text{Eq. S9}]$$

792 Finally, since the scaling factor  $\mu$  is linearly proportional to the size of the diffusing particle  $d_p$ ,  
793 we can write an expression that explicitly acknowledges particle size:

$$794 \quad V = \frac{k_2\phi^2 E_{tot}[1]S[1]}{\frac{k_{-1}[1]e^{-ad_p(\phi-1)} + k_2 + \phi S[1]}{k_1[1]e^{-ad_p(\phi-1)}}}, \quad [\text{Eq. S10}]$$

795 where  $a$  is a new scaling factor that relates  $d_p$  to  $\mu$ . Eq. S10 describes how the rate of a  
796 Michaelis-Menten reaction whose reactants obey Phillies's law and the Smoluchowski equation  
797 would be expected to vary with the cytoplasmic macromolecule concentration and molecular  
798 diameter.

799

800

801

802

803 We do not have experimental estimates for most of the parameters in Eq. S10 (except for  $a$ ,  
804 which, from Figure 4F is  $0.018 \text{ nm}^{-1}$ ) for either translation or protein degradation. However, we  
805 can get a feel for Eq. S10 by arbitrarily assuming some parameter values ( $E_{tot}[1] = S[1] =$   
806  $k_1[1] = k_{-1}[1] = k_2[1] = 1$ ) and plotting  $V$  as a function of  $\phi$  for macromolecules of different  
807 assumed macromolecular diameters. The equation defines a biphasic, non-monotonic curve  
808 (Figure S3A), and the larger the assumed macromolecular radius, the further to the left the  
809 curve's maximum lies (Figure S3B). The observed rates for translation and degradation are fairly  
810 well captured by assuming that the relevant macromolecules are 78 nm for translation and 0 nm  
811 for degradation (Figure S3C).

812

### 813 **References**

- 814 1. Phillies, G.D. (1986). Universal scaling equation for self-diffusion by macromolecules in  
815 solution. *Macromolecules* *19*, 2367-2376.
- 816 2. Phillies, G.D.J. (1988). Quantitative prediction of  $\alpha$  in the scaling law for self-diffusion.  
817 *Macromolecules* *21*, 3101-3106.
- 818 3. Smoluchowski, M. (1917). Mathematical theory of the kinetics of the coagulation of  
819 colloidal solutions. *Zeitschrift für Physikalische Chemie* *92*, 129-168.

820

821

822

## 823 References

- 824 1. Afanar, O., Buss, G.K., Stearns, T., and Ferrell, J.E., Jr. (2020). The nucleus serves as  
825 the pacemaker for the cell cycle. *Elife* 9, e59989.
- 826 2. Alric, B., Formosa-Dague, C., Dague, E., Holt, L.J., and Delarue, M. (2022).  
827 Macromolecular crowding limits growth under pressure. *Nature Physics* 18, 411-416.
- 828 3. Amodeo, A.A., Jukam, D., Straight, A.F., and Skotheim, J.M. (2015). Histone titration  
829 against the genome sets the DNA-to-cytoplasm threshold for the *Xenopus* midblastula  
830 transition. *Proc Natl Acad Sci U S A* 112, E1086-1095.
- 831 4. Aoki, K., Takahashi, K., Kaizu, K., and Matsuda, M. (2013). A quantitative model of  
832 ERK MAP kinase phosphorylation in crowded media. *Sci Rep* 3, 1541.
- 833 5. Bar-Even, A., Noor, E., Savir, Y., Liebermeister, W., Davidi, D., Tawfik, D.S., and Milo,  
834 R. (2011). The moderately efficient enzyme: evolutionary and physicochemical trends  
835 shaping enzyme parameters. *Biochemistry* 50, 4402-4410.
- 836 6. Chang, J.B., and Ferrell, J.E., Jr. (2013). Mitotic trigger waves and the spatial  
837 coordination of the *Xenopus* cell cycle. *Nature* 500, 603-607.
- 838 7. Chang, J.B., and Ferrell, J.E., Jr. (2018). Robustly Cycling *Xenopus laevis* Cell-Free  
839 Extracts in Teflon Chambers. *Cold Spring Harb Protoc* 2018, pdb.prot097212.
- 840 8. Cheng, X., and Ferrell, J.E., Jr. (2019). Spontaneous emergence of cell-like organization  
841 in *Xenopus* egg extracts. *Science* 366, 631-637.
- 842 9. Davidi, D., Noor, E., Liebermeister, W., Bar-Even, A., Flamholz, A., Tummler, K.,  
843 Barenholz, U., Goldenfeld, M., Shlomi, T., and Milo, R. (2016). Global characterization  
844 of in vivo enzyme catalytic rates and their correspondence to in vitro  $k_{cat}$  measurements.  
845 *Proc Natl Acad Sci U S A* 113, 3401-3406.
- 846 10. Delarue, M., Brittingham, G.P., Pfeffer, S., Surovtsev, I.V., Pinglay, S., Kennedy, K.J.,  
847 Schaffer, M., Gutierrez, J.I., Sang, D., Poterewicz, G., *et al.* (2018). mTORC1 Controls  
848 Phase Separation and the Biophysical Properties of the Cytoplasm by Tuning Crowding.  
849 *Cell* 174, 338-349 e320.
- 850 11. Dill, K.A., Ghosh, K., and Schmit, J.D. (2011). Physical limits of cells and proteomes.  
851 *Proc Natl Acad Sci U S A* 108, 17876-17882.

- 852 12. Drenckhahn, D., and Pollard, T.D. (1986). Elongation of actin filaments is a diffusion-  
853 limited reaction at the barbed end and is accelerated by inert macromolecules. *Journal of*  
854 *Biological Chemistry* *261*, 12754-12758.
- 855 13. Dunphy, W.G., Brizuela, L., Beach, D., and Newport, J. (1988). The *Xenopus cdc2*  
856 protein is a component of MPF, a cytoplasmic regulator of mitosis. *Cell* *54*, 423-431.
- 857 14. Elowitz, M.B., Surette, M.G., Wolf, P.E., Stock, J.B., and Leibler, S. (1999). Protein  
858 mobility in the cytoplasm of *Escherichia coli*. *Journal of bacteriology* *181*, 197-203.
- 859 15. Fang, F., and Newport, J.W. (1991). Evidence that the G1-S and G2-M transitions are  
860 controlled by different *cdc2* proteins in higher eukaryotes. *Cell* *66*, 731-742.
- 861 16. Ferrell, J.E., Jr. (1999). *Xenopus* oocyte maturation: new lessons from a good egg.  
862 *Bioessays* *21*, 833-842.
- 863 17. Fox, C.A., Sheets, M.D., and Wickens, M.P. (1989). Poly(A) addition during maturation  
864 of frog oocytes: distinct nuclear and cytoplasmic activities and regulation by the sequence  
865 UUUUUAU. *Genes Dev* *3*, 2151-2162.
- 866 18. Garner, R.M., Molines, A.T., Theriot, J.A., and Chang, F. (2023). Vast heterogeneity in  
867 cytoplasmic diffusion rates revealed by nanorheology and Doppelganger simulations.  
868 *Biophys J* *122*, 767-783.
- 869 19. Gires, P.-Y., Thampi, M., Krauss, S.W., and Weiss, M. (2023). Exploring generic  
870 principles of compartmentalization in a developmental in vitro model. *Development* *150*.
- 871 20. Green, S.L. (2009). *The laboratory Xenopus sp*, 1 edn (CRC Press).
- 872 21. Hu, X.P., Dourado, H., Schubert, P., and Lercher, M.J. (2020). The protein translation  
873 machinery is expressed for maximal efficiency in *Escherichia coli*. *Nat Commun* *11*,  
874 5260.
- 875 22. Huang, W.Y.C., Cheng, X., and Ferrell, J.E., Jr. (2022). Cytoplasmic organization  
876 promotes protein diffusion in *Xenopus* extracts. *Nat Commun* *13*, 5599.
- 877 23. Jin, M., Tavella, F., Wang, S., and Yang, Q. (2022). In vitro cell cycle oscillations exhibit  
878 a robust and hysteretic response to changes in cytoplasmic density. *Proc Natl Acad Sci U*  
879 *S A* *119*, e2109547119.
- 880 24. Kamenz, J., Qiao, R., Yang, Q., and Ferrell, J.E., Jr. (2021). Real-Time Monitoring of  
881 APCAnaphase-promoting complex (APC)/C-Mediated Substrate Degradation Using

- 882           *Xenopus laevis* Egg Extracts. In Cell Cycle Oscillators : Methods and Protocols, A.S.  
883           Coutts, and L. Weston, eds. (New York, NY: Springer US), pp. 29-38.
- 884       25. Kanki, J.P., and Newport, J.W. (1991). The cell cycle dependence of protein synthesis  
885           during *Xenopus laevis* development. *Dev Biol* 146, 198-213.
- 886       26. King, R.W., Deshaies, R.J., Peters, J.M., and Kirschner, M.W. (1996). How proteolysis  
887           drives the cell cycle. *Science* 274, 1652-1659.
- 888       27. Klumpp, S., Scott, M., Pedersen, S., and Hwa, T. (2013). Molecular crowding limits  
889           translation and cell growth. *Proc Natl Acad Sci U S A* 110, 16754-16759.
- 890       28. Liu, X., Oh, S., and Kirschner, M.W. (2022). The uniformity and stability of cellular  
891           mass density in mammalian cell culture. *Front Cell Dev Biol* 10, 1017499.
- 892       29. Liu, X., Oh, S., Peshkin, L., and Kirschner, M.W. (2020). Computationally enhanced  
893           quantitative phase microscopy reveals autonomous oscillations in mammalian cell  
894           growth. *Proc Natl Acad Sci U S A* 117, 27388-27399.
- 895       30. Meneau, F., Dupre, A., Jesus, C., and Daldello, E.M. (2020). Translational Control of  
896           *Xenopus* Oocyte Meiosis: Toward the Genomic Era. *Cells* 9, 1502.
- 897       31. Milo, R., Jorgensen, P., Moran, U., Weber, G., and Springer, M. (2009). BioNumbers—  
898           the database of key numbers in molecular and cell biology. *Nucleic Acids Research* 38,  
899           D750-D753.
- 900       32. Minshull, J., Blow, J.J., and Hunt, T. (1989). Translation of cyclin mRNA is necessary  
901           for extracts of activated *Xenopus* eggs to enter mitosis. *Cell* 56, 947-956.
- 902       33. Minton, A.P. (2001). The influence of macromolecular crowding and macromolecular  
903           confinement on biochemical reactions in physiological media. *The Journal of biological*  
904           *chemistry* 276, 10577-10580.
- 905       34. Mitchison, T.J., and Field, C.M. (2021). Self-Organization of Cellular Units. *Annu Rev*  
906           *Cell Dev Biol* 37, 23-41.
- 907       35. Molines, A.T., Lemiere, J., Gazzola, M., Steinmark, I.E., Edrington, C.H., Hsu, C.T.,  
908           Real-Calderon, P., Suhling, K., Goshima, G., Holt, L.J., *et al.* (2022). Physical properties  
909           of the cytoplasm modulate the rates of microtubule polymerization and depolymerization.  
910           *Dev Cell* 57, 466-479 e466.
- 911       36. Murray, A., W. (1991). Cell Cycle Extracts. In *Methods in Cell Biology*, Brian K. Kay,  
912           and H.B. Peng, eds. (Academic Press), pp. 581-605.

- 913 37. Murray, A.W., and Kirschner, M.W. (1989). Cyclin synthesis drives the early embryonic  
914 cell cycle. *Nature* 339, 275-280.
- 915 38. Neurohr, G.E., and Amon, A. (2020). Relevance and Regulation of Cell Density. *Trends*  
916 *in cell biology* 30, 213-225.
- 917 39. Newport, J., and Kirschner, M. (1982a). A major developmental transition in early  
918 *Xenopus* embryos: I. characterization and timing of cellular changes at the midblastula  
919 stage. *Cell* 30, 675-686.
- 920 40. Newport, J., and Kirschner, M. (1982b). A major developmental transition in early  
921 *Xenopus* embryos: II. Control of the onset of transcription. *Cell* 30, 687-696.
- 922 41. Newport, J., and Spann, T. (1987). Disassembly of the nucleus in mitotic extracts:  
923 membrane vesicularization, lamin disassembly, and chromosome condensation are  
924 independent processes. *Cell* 48, 219-230.
- 925 42. Oh, S., Lee, C., Yang, W., Li, A., Mukherjee, A., Basan, M., Ran, C., Yin, W., Tabin,  
926 C.J., Fu, D., *et al.* (2022). Protein and lipid mass concentration measurement in tissues by  
927 stimulated Raman scattering microscopy. *Proc Natl Acad Sci U S A* 119, e2117938119.
- 928 43. Paris, J., Osborne, H.B., Couturier, A., Le Guellec, R., and Philippe, M. (1988). Changes  
929 in the polyadenylation of specific stable RNA during the early development of *Xenopus*  
930 *laevis*. *Gene* 72, 169-176.
- 931 44. Peshkin, L., Wuhr, M., Pearl, E., Haas, W., Freeman, R.M., Jr., Gerhart, J.C., Klein,  
932 A.M., Horb, M., Gygi, S.P., and Kirschner, M.W. (2015). On the Relationship of Protein  
933 and mRNA Dynamics in Vertebrate Embryonic Development. *Dev Cell* 35, 383-394.
- 934 45. Phillies, G.D. (1986). Universal scaling equation for self-diffusion by macromolecules in  
935 solution. *Macromolecules* 19, 2367-2376.
- 936 46. Phillies, G.D.J. (1988). Quantitative prediction of  $\alpha$  in the scaling law for self-diffusion.  
937 *Macromolecules* 21, 3101-3106.
- 938 47. Richter, K., Nessling, M., and Lichter, P. (2007). Experimental evidence for the influence  
939 of molecular crowding on nuclear architecture. *Journal of cell science* 120, 1673-1680.
- 940 48. Rosenthal, E.T., Tansey, T.R., and Ruderman, J.V. (1983). Sequence-specific  
941 adenylations and deadenylations accompany changes in the translation of maternal  
942 messenger RNA after fertilization of *Spisula* oocytes. *J Mol Biol* 166, 309-327.

- 943 49. Ruderman, J.V., Woodland, H.R., and Sturgess, E.A. (1979). Modulations of histone  
944 messenger RNA during the early development of *Xenopus laevis*. *Dev Biol* 71, 71-82.
- 945 50. Schwanhausser, B., Busse, D., Li, N., Dittmar, G., Schuchhardt, J., Wolf, J., Chen, W.,  
946 and Selbach, M. (2011). Global quantification of mammalian gene expression control.  
947 *Nature* 473, 337-342.
- 948 51. Scott, M., Klumpp, S., Mateescu, E.M., and Hwa, T. (2014). Emergence of robust growth  
949 laws from optimal regulation of ribosome synthesis. *Mol Syst Biol* 10, 747.
- 950 52. Smith, L.D., Xu, W.L., and Varnold, R.L. (1991). Oogenesis and oocyte isolation.  
951 *Methods Cell Biol* 36, 45-60.
- 952 53. Smoluchowski, M. (1917). Mathematical theory of the kinetics of the coagulation of  
953 colloidal solutions. *Zeitschrift für Physikalische Chemie* 92, 129-168.
- 954 54. Son, S., Kang, J.H., Oh, S., Kirschner, M.W., Mitchison, T.J., and Manalis, S. (2015).  
955 Resonant microchannel volume and mass measurements show that suspended cells swell  
956 during mitosis. *Journal of Cell Biology* 211, 757-763.
- 957 55. Tan, C., Saurabh, S., Bruchez, M.P., Schwartz, R., and Leduc, P. (2013). Molecular  
958 crowding shapes gene expression in synthetic cellular nanosystems. *Nat Nanotechnol* 8,  
959 602-608.
- 960 56. Zimmerman, S.B., and Trach, S.O. (1991). Estimation of macromolecule concentrations  
961 and excluded volume effects for the cytoplasm of *Escherichia coli*. *J Mol Biol* 222, 599-  
962 620.
- 963 57. Zlotek-Zlotkiewicz, E., Monnier, S., Cappello, G., Le Berre, M., and Piel, M. (2015).  
964 Optical volume and mass measurements show that mammalian cells swell during mitosis.  
965 *Journal of Cell Biology* 211, 765-774.  
966